Journal of Sound and Vibration (1978) 57(3), 389-402

STUDIES ON VIBRATION OF SOME RIB-STIFFENED CANTILEVER PLATES

M. N. BAPU RAO, P. GURUSWAMY, M. VENKATESHWARA RAO AND S. PAVITHRAN

Structural Sciences Division, National Aeronautical Laboratory, Bangalore-560017, India

(Received 15 August 1977, and in revised form 29 November 1977)

An experimental study was carried out to determine the resonant mode shapes and frequencies of some rib-stiffened skew cantilever plates by holographic interferometry. The influences of varying the sweep back angle, the rib stiffness and the aspect ratio, and the effect of varying the boundary conditions at the root chord, on the frequencies and mode shapes were also investigated. Results of the above investigation and also those of a comparative study with the finite element solution obtained for some of the cases studied are presented and discussed.

1. INTRODUCTION

Rib-stiffened skew plates are commonly employed in the structures of many aerospace vehicles such as missiles, rockets and aircraft. It is therefore necessary to determine the vibration characteristics of such structures for design purposes. While extensive investigations have been carried out in respect to unstiffened plates, similar studies regarding the stiffened plates appear to have been made on a relatively smaller scale. For brevity only a few of them will be mentioned here.

Lindberg and Olson [1] carried out response studies of a multi-bay panel system under random input, by using finite element methods. They also determined the vibration characteristics of an integrally stiffened panel subjected to a jet noise excitation [2]. Yurkovich *et al.* [3] carried out dynamic analysis of stiffened all round supported rectangular panel structures by both experimental and theoretical methods. Recently Durvasula [4] presented the results of his studies on the vibration problem of shaft-supported low aspect ratio wing-type structures. Various stiffened configurations were investigated by considering different combinations of the plate, the spar and the ribs. More recently Olson and Hazell [5] reported on the vibrational behaviour of stiffened square plates with all round fixed boundaries, as observed by holographic interferometric techniques. Very good experimental results in respect to mode shapes and frequencies, which were also in good agreement with those of theory, were obtained. But to the best knowledge of the present investigators, results of intensive studies on the vibrational characteristics of rib-stiffened cantilever skew plates have so far not been published.

In this paper, vibrational mode shapes and frequencies for some rib-stiffened skew cantilever plates, as determined by holographic interferometry, are presented. Effects of varying the sweepback angle, the rib stiffness and the aspect ratio, and also the effect of varying root-chord boundary conditions arising from the introduction of cuts at the root at different locations and of varying extents, on the vibrational behaviour of the plates have also been investigated. The purpose of this investigation was to carry out these parametric studies of stiffened plates in order to gain insight into their vibrational behaviour that is needed in the design of actual structures. In addition, it is appropriate to mention here that in the design of many guided rockets and missiles the edges are clamped over only a part of the root chord; or alternatively the root support may consist of a bending and shear-resisting

0022-460X/78/0408-0389$02.00/0

hub at the mid-chord point and a shear-resisting pin at some other point away from the hub along the root. For such situations the results of the present investigation on the effects of the cuts introduced at the root chord can provide useful data for gaining better understanding as to their vibrational behaviour.

Resonant frequencies were determined by the quadrature method in conjunction with a cathode ray oscilloscope and the associated modes by the time-averaged holographic method. Real time holographic interferometry can provide extremely accurate values for resonant frequencies, and mode missing can seldom occur with this technique. This technique, which was developed in the later stages of the present investigation, was employed for studying only a few of the cases considered for vibration testing. In addition, calculated results for some cases were obtained by the finite element method. Results from the theoretical and experimental comparison study are presented for all cases studied and discussed.

2. HOLOGRAPHIC INTERFEROMETRY

Resonant mode shapes are determined by using time-averaged holographic interferometry, in which interference between images corresponding to two peak displacement positions of a vibrating object is obtained in a single exposure. In this method the exposure time is much longer than the period of oscillation of the vibrating object. The holographic plate is exposed to the scattered light from the vibrating object in each position the object assumes during exposure. However the hologram formed will record most densely the reflected wave fronts corresponding to the peak displacement positions (zero velocity positions) in which the object spends most of the exposure time interval. On reconstruction the hologram displays the stationary nodal areas brightly as in the normal hologram, but the antinodes are seen contoured by fringes of equal displacement [6].

In the real time holographic technique a hologram of the object in its unloaded state is first recorded and processed *in situ*. The reconstructed wave front of the object is then allowed to interfere with the light scattered by the object subjected to vibration; the resulting interference pattern represents the nodal and anti-nodal regions of the vibrating object.

2.1. EXCITATION AND DETERMINATION OF NATURAL FREQUENCIES

The natural frequencies were determined by conducting a resonance test, the excitation equipment consisting of an electronic oscillator, 60 W power amplifier and an acoustic exciter, in conjunction with a cathode-ray oscilloscope (CRO).

The response was measured through the use of a magnetic pick-up which was moved around to ensure that no mode was missed on account of the pick-up being close to or in nodal areas.

Natural frequencies were determined by using the principle of Lissajous figures, in which a comparison is made of the phases of the exciting force and response in the CRO. When a structure with small damping and well-separated natural frequencies is considered, the natural frequency of vibration can be taken to be represented by that frequency of excitation at which the phase difference between the force and displacement is 90°. This technique of determining the resonant frequency was employed in association with the time-averaged holography which was used for the determination of associated mode shapes.

The quadrature response method, as employed in the present study, has been chosen in preference to the far more accurate Kennedy Pancu technique in view of the simplicity and rapidity with which the frequencies can be determined in the former case with reasonable accuracy.

For the real time holography, excitation of the object was carried out as described above. However, in this case it was not necessary to monitor the response by using the oscilloscope. Instead the resonant frequencies were determined by the observation of live interference

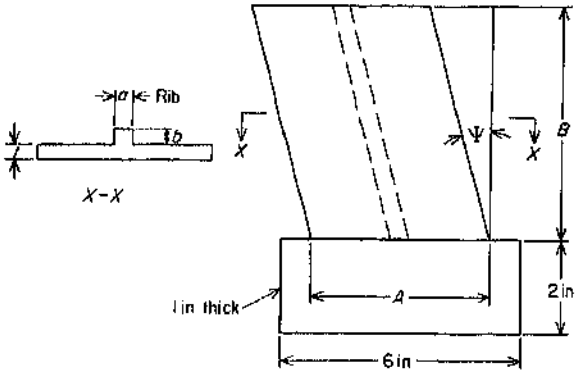

Figure 1. Structural details of the rib-stiffened plate model.

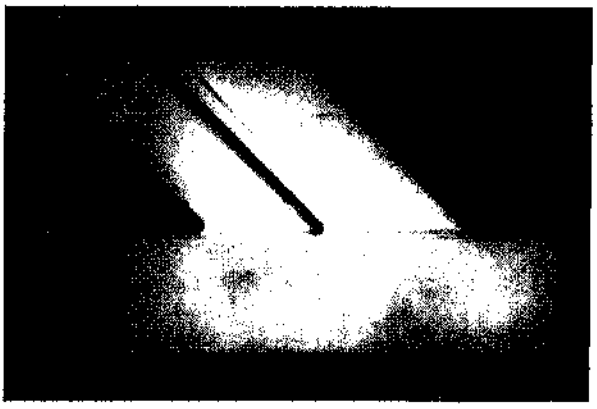

Figure 2. Integrally machined plate model with a rib.

fringes obtained by the vibration of the object, which become stationary and sharp whenever the oscillator is tuned to a resonant frequency. The amplitude of vibration can then be adjusted to the desired fringe distribution which represents the nodal and anti-nodal regions of the associated mode shapes. In this method all resonant frequencies can be scanned with just one hologram,

The resonant frequencies were recorded with the aid of a frequency counter.

In order to obtain realistic experimental conditions the rib-stiffened plate models as employed in the test were integrally machined from 1 inch thick mild steel plates, with the

TABU! 1

Structural and material properties of rib-stiffened plates

Case	Plate dimension A x B (mm)	Thickness of the plate, t (mm)	Rib dimension (mm)	Sweep back angle Ψ (degrees)
1	114x114	2	6·35 x 6·35	0
2a	114 x 114	2	6·35 x 6·35	30
2b	114 × 114	2	4·76 x 8·45	30
2c	114 x 114	2	3·18 x 12·7	30
3a	114 x 114	2	6·35 x 6·35	45
3b	114 × 114	2	4·76 x 8·45	45
3c	114 x 114	2	3·18 × 12·7	45
3d	114 × 76	2	6·35 x 6·35	45

Material mild steel, $E = 2{\cdot}068 \times 10^{11} \mathrm{N/m^2}$, $\nu = 0{\cdot}3$.

thick flat portion at the root retained. (See Figures 1 and 2), and the models were rigidly fixed in a vice such that the entire surface area of the flat portion at the root was in contact with the jaws of the vice; by this method of fixing the possibility of rigid body motions of the object during testing can be completely eliminated. Figure 1 shows the details of the model construction. The structural and material properties of the plate specimens as employed in the present investigation are given in Table 1.

2.2. EXPERIMENTAL PROCEDURE

Figure 3 shows a schematic presentation of a typical arrangement of carrying out the experiments. The diagram displays a 50 mW Helium-Neon laser (Spectral Physics) representing the monochromatic coherent light source and vibration-isolated steel table. The associated optical components which are held in position, on the table are also shown in the same figure.

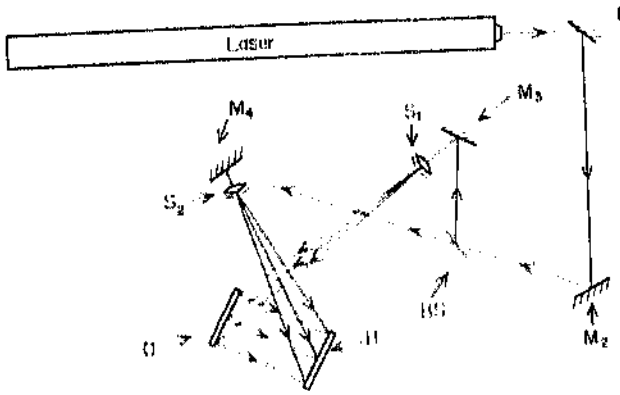

Figure 3. Schematic diagram of the holographic set-up. H, holographic plate; O, object; BS, beam splitter; S_1, S_2, spatial filters; M_1, M_2, M_3, M_4, plane mirrors.

The object under investigation and the hologram plate holder in which the holographic plate was inserted were placed in the required position. The object and reference beams were then directed to the surfaces of the object and the photographic plate, respectively. The object to be tested was excited to its natural frequencies and the desired time-averaged holograms obtained after taking the usual precautions necessary in a holographic interferometric technique.

The ratio of intensities of the object and reference beams at the holographic plate was maintained approximately at $\frac{1}{8}$ in recording time-averaged holograms. The holographic plates employed were Kodak 120-02's and processing was carried out with D-19b developer. Typical exposure times ranged between 10-20 seconds.

3. THEORETICAL CONSIDERATIONS

In order to carry out a comparative study with the experimental results a theoretical solution to the problem was also obtained by the finite element method.

The plates were structurally idealized by using triangular elements with three nodes, each node being associated with three degrees of freedom: namely, the lateral displacement W, and the rotations about the x and y axes, $\partial W/\partial x$ and $\partial W/\partial y$. The ribs were idealized by using beam elements with three corresponding compatible degrees of freedom. The displacement W is described by a cubic polynomial function in the (x, y) co-ordinates. A total of 128 elements with 81 nodes was employed in the idealization.

The stiffness and mass matrices were generated globally, the order of the matrices being reduced by a condensation procedure eliminating the rotational degrees of freedom. Eigenfrequencies and vectors were then determined through standard numerical procedures.

4. RESULTS AND DISCUSSION

Table 2 shows the experimental values of the frequencies for the cases 1, 2a and 3a, corresponding to the rib size 6·35 x 6·35, obtained by the quadrature method for the time-averaged holography. In order to avoid confusion in distinguishing the results obtained by the quadrature and real time methods, in our further discussion the terms "experimental results" must be considered to mean those obtained by the quadrature method for the time-averaged holography. Finite element results obtained for the cases V = 30° and 45°, and the frequency values as determined by the real time holographic method for the case Ψ = 45° are also

TABLE 2

Effect of sweep back angle on the frequencies (Hz)

Case 1 $\Psi = 0°$	Case 2a $\Psi = 30°$		Case 3a $\Psi = 45°$	
E	E	T	E	T
115	160	169	180 (190)	165
237	355	384	420 (400)	382
682	831	897	860 (850)	783
882	893	978	1090 (1040)	992
1178	1257	1332	1580 (1605)	1545
1545	1630	1790	1755 (1730)	1731
1900	2000	2170	2135 (2180)	2163

E: Experimental; T: Theoretical.

given in the same table; for the real time case the values are given in the parentheses. It can be seen that the agreement between the experimental and theoretical results is reasonably good. While the percentage difference between the two sets of results for Ψ = 45° varies from 1·3 to 9 the corresponding percentage values for the case Ψ = 30° ranges from a maximum of 9·0 to 5·45. However, the frequency values as given by the real time holographic technique, which must be considered more accurate than either of the other two methods, are closer to those of theory except for the first and fifth modes. For Ψ = 0° the theoretical results are not available; therefore no comparison can he made. Good agreement between the theoretically and experimentally determined mode shapes are also found for the cases Ψ = 30° and 45°, as can be observed from Figures 4 to 7 which display modes 2 to 7. The fundamental modes, which turn out to be cantilever bending modes, corresponding to f = 160 Hz (Ψ = 30°) and f = 180 Hz (Ψ = 45°) are not shown in these figures. The corresponding time-averaged holograms are also shown in the same figures (on the right side); in these holograms the bright fringes represent nodal lines while other fringes depicting contours of equal amplitudes represent antinodal regions. The full lines representing experimentally determined nodal lines (as shown on the left side of these figures) correspond to bright nodal lines as given in the holograms and in fact are reproduced from the latter. It can be noticed from these figures that modes 2, 4 and 6 for Ψ = 30° and modes 2, 4 and 7 for Ψ = 45° exhibit similarity in shapes to some extent. It may also be observed from the hologram for mode 4

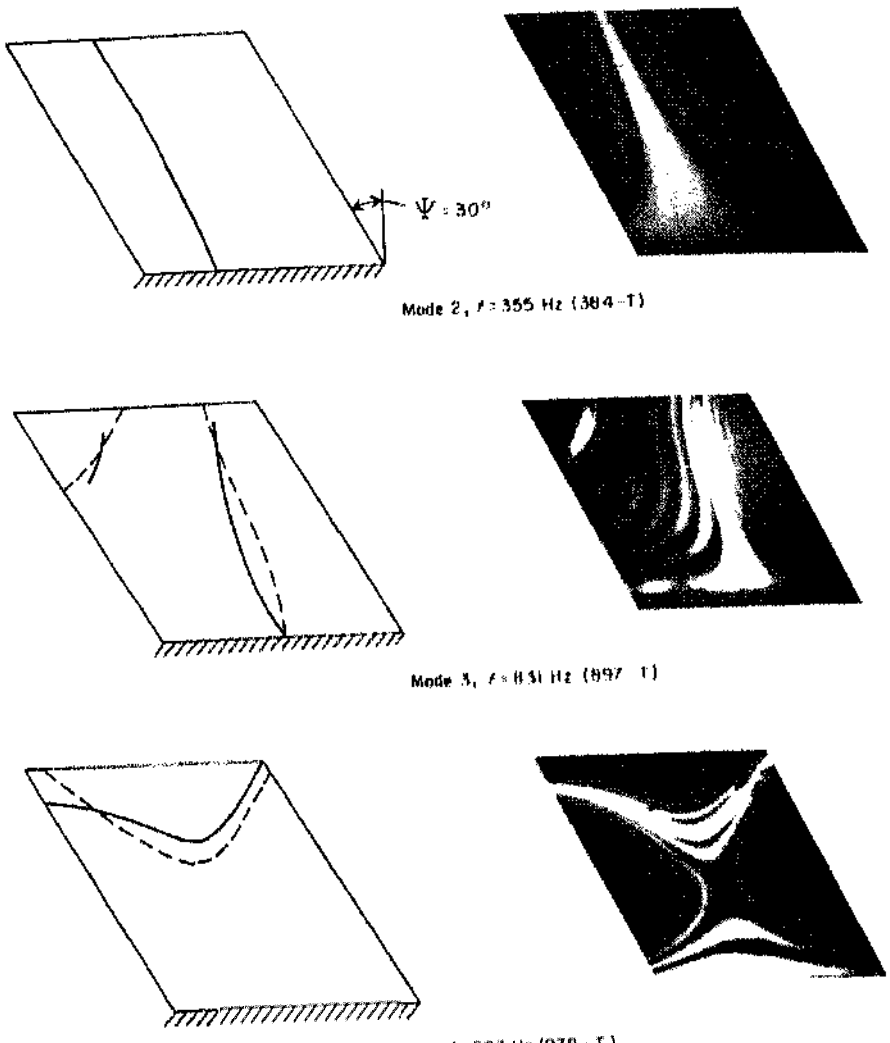

Figure 4. Comparison of experimental and theoretical nodal patterns. Ψ 30" (ease 2a). ——, Experimental;.....—, theoretical,

that apart from the bright nodal line a, the root another white fringe appears immediately following the first dark fringe; this additional white ringe does not represent a node although i, appears to be quite bright; this was inferred from the observation of the actual hologram. No significant remarks can be made in respect of othc modes. Figt shows modes1 to 6 for the case V 0". It may be remarked here that while some similar tyi mole shape can be observed between the cases Ψ 30" and 4V. I ie mode l$_u$ cs co pondi g to $\Psi = 0°$ appear U, he completely different from those of the former case ex pt for three modes, which are similar U. the first, second and fourth modes for cases ψ)° and 45° (sec Figures 4, (i and 8).

The effect of varying the rib stiffnesses with their masses k p. reconstruit's considered next. Table 3 shows the experimental and theoretical results fo e I equencies forth late with ψ .45°, stiffened with rihx of different cross-sections (ci es 3; 3c . 3b only theoretical results are presented. In all the three cases the :t) c the pl mass i maintained constant. The percentage difference between he theoretic imenta results for case 3c is found lo vary between a maximum of 8·77 to a very mall value. Cas U. a

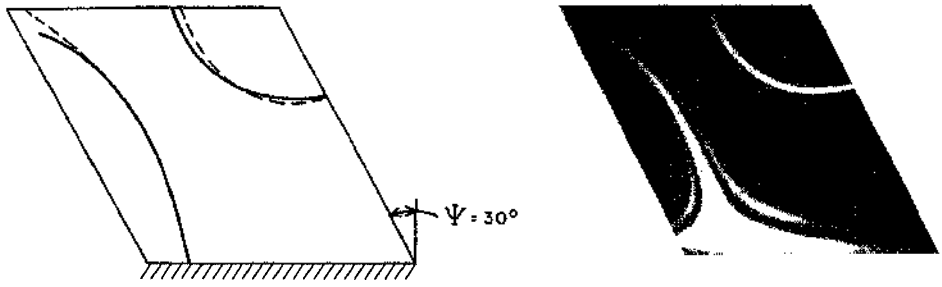

Mode 5, f = 1257 Hz (1332 – T)

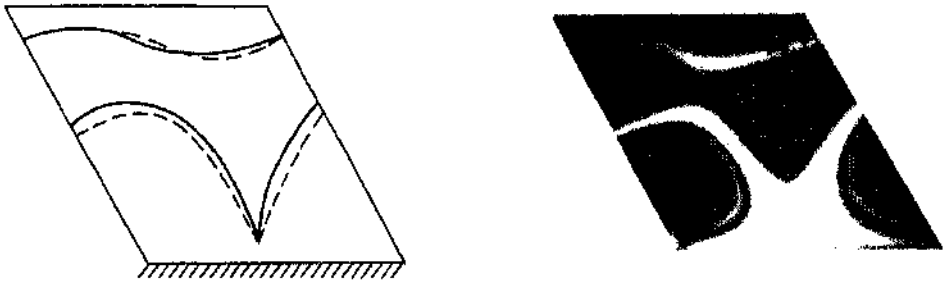

Mode 6, f = 1630 Hz (1790 – T)

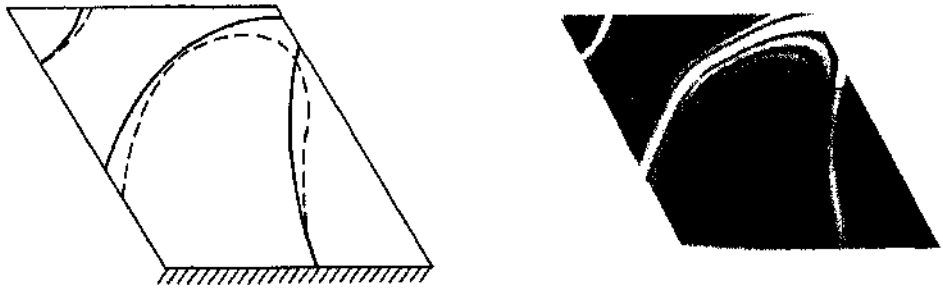

Mode 7, f = 2000 Hz (2170 – T)

Figure 5. Comparison of experimental and theoretical nodal patterns. $\Psi = 30°$ (case 2a). ——, Experimental; – – – –, theoretical,

3a has already been considered earlier. As for the mode shapes, only minor changes are observed when the results corresponding to eases 3a and 3b are compared; the mode shapes for the latter are therefore not presented to save space. For case 3c, it is interesting to note that the third mode deviates to some extent from the corresponding third one of case 3a (see Figure 9) but follows somewhat closely the third mode of $\Psi = 30°$ (case 2a), while only minor changes can be observed with regard to other modes, with absolutely no change in sequence in comparison with those of case 3a; other mode shapes for case 3c are therefore not presented.

For the plate with Ψ = 30°, the corresponding variation of rib stiffness (cases 2a-2c) seems to have only a small influence on the mode shapes without any accompanying changes in sequence; the mode shapes for the cases 2b and 2e are therefore not presented to save space. The only change brought about is the expected increase in frequencies following the

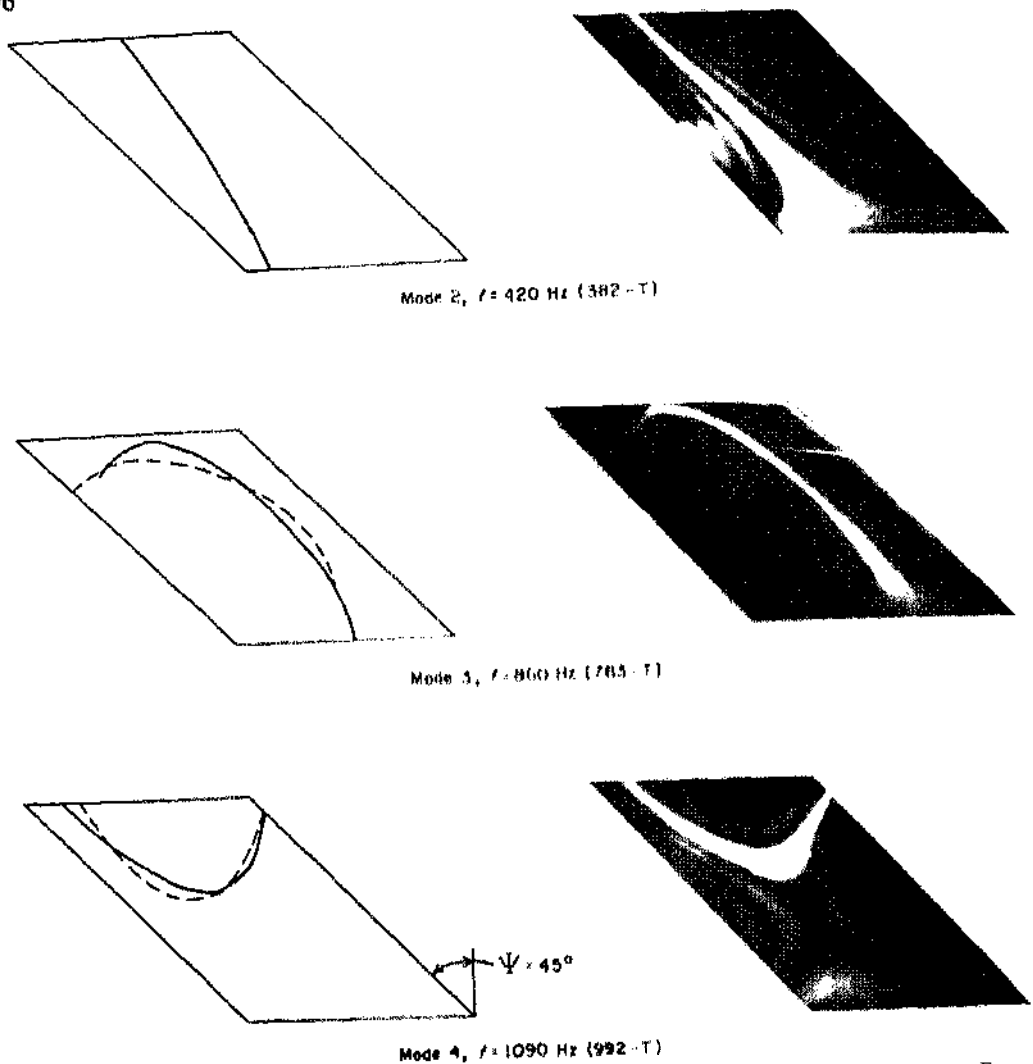

Figure 6. Comparison of experimental and theoretical nodal patterns. $\Psi = 45°$ (case 3a). - - -, Experimental; ———, theoretical.

increase of stiffnesses as can be seen in Table 4, cases 2a 2c. For the cases 2b and 2c frequencies were not determined experimentally and therefore only finite element results are presented, The results for case 2a have already been discussed.

The influence of varying the aspect ratio on resonant frequencies and mode shapes is considered next, Reduction of the aspect ratio, as represented by case 3d, produces an increase in frequencies as expected and as Known in Table 5. The fourth mode for this case, $\Psi = 45°$, appears as shown in Figure 10 (left) with f 1763 Hz. As can be observed, there is considerable deviation from the corresponding one of case 3a (Figure 10, right), Other than this departure, only minor changes take place in respect of other mode shapes, the sequence of modes remaining unaltered, Similar remarks can be made in respect of V = 30° also; results for this case are not presented to save space.

Introduction of cuts at the root alters the boundary condition along the base width, thereby causing variation in the behaviour of the structure, the magnitude and type of changes depending upon the location and extent of cuts introduced. This part of the investigation is discussed next. The extent and location of cuts considered are shown in figure 11. The

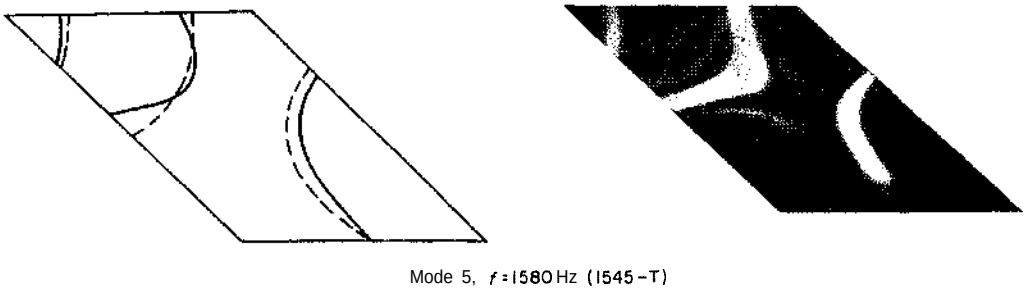

Mode 5, f = 1580 Hz (1545 – T)

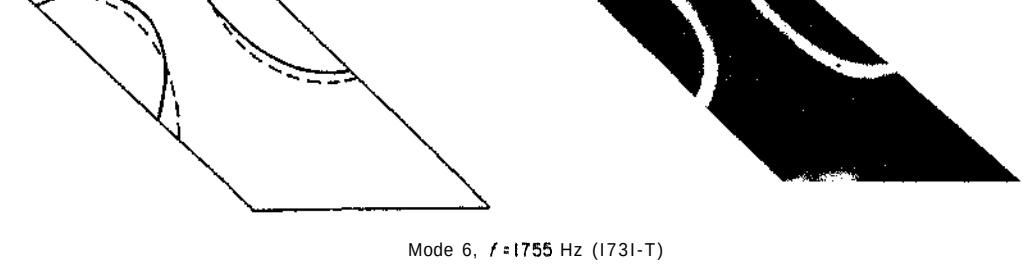

Mode 6, f = 1755 Hz (1731-T)

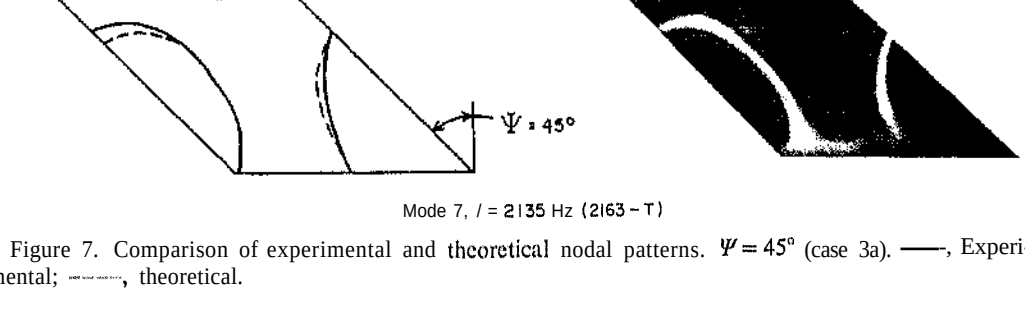

Mode 7, / = 2135 Hz (2163 – T)

Figure 7. Comparison of experimental and theoretical nodal patterns. $\Psi = 45^{\circ}$ (case 3a). ——, Experimental; – – – –, theoretical.

resonant frequencies for cases A, B and C corresponding to various cuts introduced at the root chord, are shown in Table 6; also shown in this table are the values for the uncut case, case 3a, for comparison purposes; the frequencies for all these cases were determined by the real time holographic method. From this table it can be seen that there is a reduction in frequencies as the extent of cuts is increased, as can be expected. The second mode associated with cases A, B and C appears to be nearly the same as that for case 3a except at the root (see Figure 12, top). For case A the nodal line along the cut (first cut introduced) disappears. For case B the mode shape remains the same as for case A indicating the existence of the root nodal line along the second cut; this shows the second cut has no influence on the mode shape. It should be noticed that the first cut producing the change in the behaviour also happens to be located at the re-entrant corner which is the region of high stress concentration. Extension of the cut all along the base except in the neighbourhood of the rib allows the nodal line to exist only along the uncut zone (see again Figure 12, top, extreme right). Almost

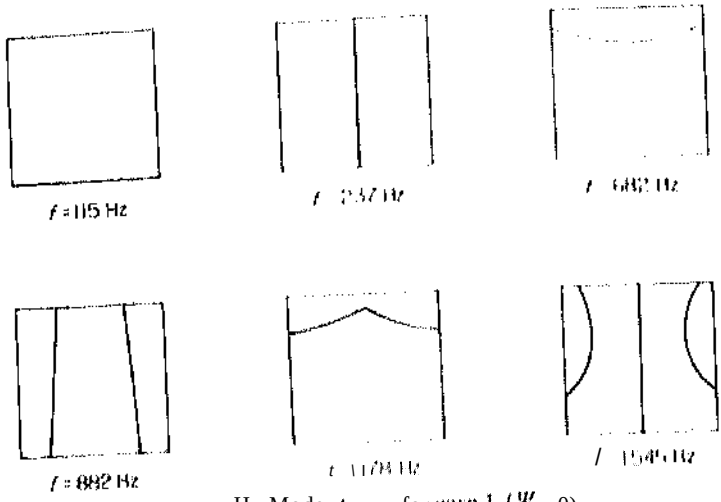

Figure H, Mode shapes for case 1, (Ψ 0).

TABLE 3

Effect of rib stiffness on the frequencies (Hz), $\Psi = 45°$

Case 3a $a \times b = 6{\cdot}35 \times 6{\cdot}35$		Case 3b $4{\cdot}76 \times 8{\cdot}45$	Case 3c $3{\cdot}18 \times 12{\cdot}7$	
E	T	T	E	T
180	165	195	285	310
420	382	465	495	503
860	783	859	961	963
1090	992	1116	1245	1272
1580	1545	1629	1750	1728
1755	1731	1799	1805	1895
2135	2163	2255		

E: Experimental; T: Theoretical.

Figure 9. Effect of varying the rib stiffness for the plate with $\Psi = 45°$, (mode 3 shown above).

TABLE 4
Effect of rib stiffness on the frequencies (Hz), $\Psi = 30°$

Case 2a 6·35 x 6·35		Case 2b 4·76 x 8·45	Case 2c 3·18 x 12·70
E	T	T	T
160	169	203	272
355	384	455	566
831	897	983	1026
893	978	1056	1146
1257	1332	1504	1541
1630	1790	2048	2281
2000	2170	2428	2528
2296	2502	2722	2959

E: Experimental; T: Theoretical.

similar behaviour is noticed for the third mode also (see Figure 12, bottom). Figure 13 shows the comparison of mode shapes for various eases of cuts considered for modes 4 to 7. The fourth mode for cases A, B and C appear to be the same as that for the uncut case except for the expected reduction in the associated frequencies due to increased flexibilities arising from the cuts introduced; the higher flexibilities also permit additional modes to

TABLE 5
Effect of aspect ratio on the frequencies (Hz), $\Psi = 45°$

Case 3a	Case 3d
180	476
420	806
860	1371
1090	1763

occur at $f = 1150$ Hz and $f = 1140$ Hz in cases B and C, respectively (the frequencies for the additional modes are given in the parentheses in Figure 13 and in Table 6). In the case of modes 5 and 6 similar behaviour can be noticed except for the fact that the modes corresponding to those for the uncut case are not present in case C; this is indicated by a sign ⊗ in Figure 13 and Table 6 at appropriate locations. The phenomenon of mode disappearance

Figure 10. Effect of varying the aspect ratio tor the plate with $\Psi = 45°$, (mode 4 shown above).

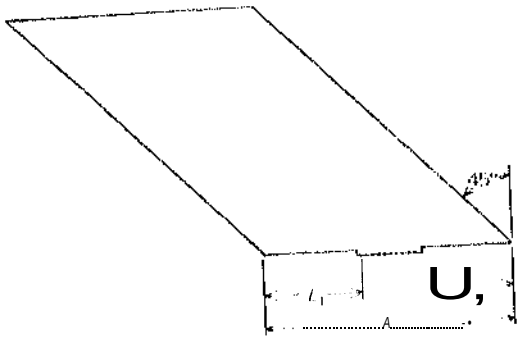

Figure 11. Dimensions of cuts at the root of the plate. Case A: L_2 0, /., 28·6 mm; case B: $L_1 = L_2 =$ 28·6 mm; case C: $L_1 = L_2 =$ 44·5 mm.

also occurs **in** the case of the 7th mode for cases B and C, followed by **the appearance** of additional modes as in the cases of he pre modes

It may be remarked in passing that differences ... a maximum of nine percent between experimentally and theoretically determined values as realized in the comparison study of

TABLE 6

Effect of cuts at the root on the frequencies (Hz), $\psi = 45°$

Case 3a	Case A	Case B	Case C
190	175	**160**	160
400	385	360	340
850	795	745	710
1040	1025	940 (1150)	905 (1140)
1605	1515	1360 (1510)	(1260)
1730	1680	1555 (1905)	(1615)
2180	2145	(2145)	(1975)

frequencies can be reduced by the following considerations. Frequencies determined from the Kennedy-Pancu technique in place of the quadrature response method can provide more accurate experimental results. Very accurate values for frequencies can also be obtained by using the real time holographic technique, as has been done for a few cases. As for the

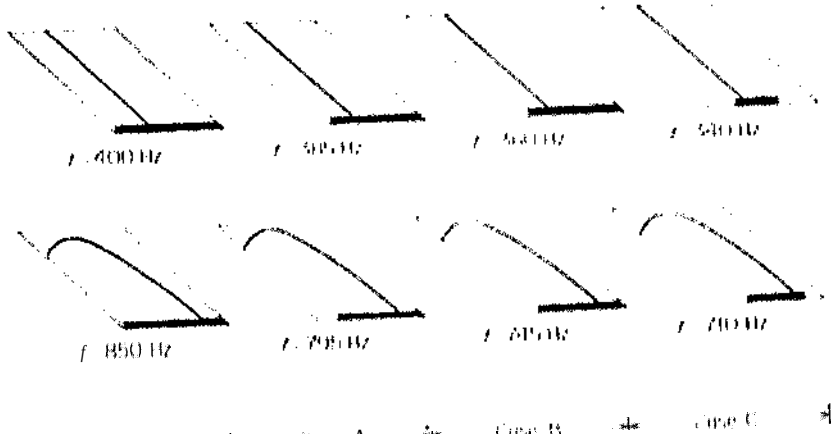

Case 3a Case A Case B Case C

Figure 12. Effect of cuts on mode shapes of the plate with ψ 45 (mode 2 at top, ... 3 t bottom). ——, Root nodal line,

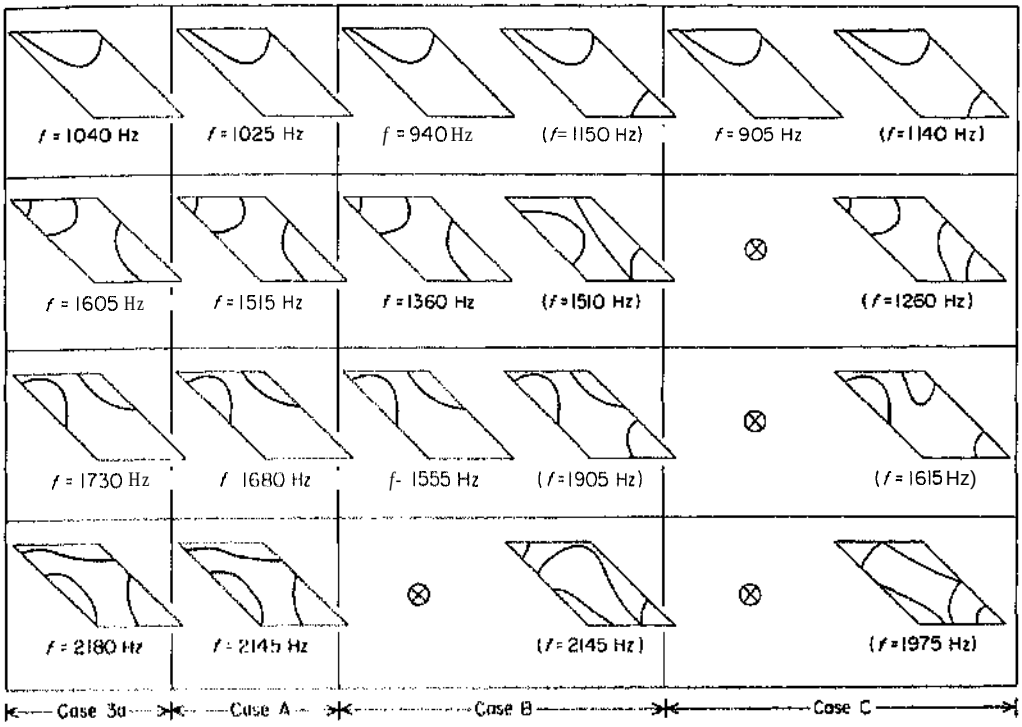

Figure 13. Effect of cuts on mode shapes of the plate with $\Psi = 45°$ (modes 4-7 from top to bottom).

theoretically determined results, simple plate and beam bending elements have been employed in the present analysis. However, use of higher order elements, in which both membrane and bending deformations associated with higher order of degrees of freedom are considered, gives rise to more accurately determined results. Inclusion of both membrane and bending plate deformations becomes more meaningful as the value of the rib depth increases for given plate sizes, especially when the value of the former approaches the order of the plate dimensions. It may be mentioned here that Olson and Hazell [5] obtained very accurate results in vibrational studies of rib-stiffened square plates through the use of high precision plate and beam elements, both membrane and bending deformation being included in the plate element. Nevertheless the present studies have provided insight into the vibrational behaviour of the various cases of rib-stiffened plates considered.

ACKNOWLEDGMENT

The authors would like to express their grateful thanks to Mr B. R. Somashekar, Head of Structures, National Aeronautical Laboratory, Bangalore, for his interest in this investigation and also to The Aeronautics Research and Development Board for the financial support provided for carrying out this investigation. The authors also wish to thank Miss J. R. Kulkarni for plotting the theoretical mode shapes,

REFERENCES

1. G. M. LINDBERG and M, D. OLSON 1967 *National Research Council of Canada Aero Report LR-492.* Vibration modes and random response of u multi-bay panel system using finite elements.
2. M, D. OLSON and G, M. LINDBERG 1971 *Journal of Aircraft* 8, 847-855. Jet noise excitation of an integrally stiffened panel.
3. R. N. YURKOVICH, J. H. SCHMIDT and A. R. ZAK 1971 *Journal of Aircraft* 8, 149-155. Dynamic analysis of stiffened panel structures.

4 S. DURVASULA 1971 *Journal of the Indian Rocket Society* **11**, 13–32. Vibration of shaft-supported low aspect ratio control surfaces.

5. M. D. OLSON and C. R. HAZELL 1977 *Journal of Sound and Vibration* 50, 43–61. Vibration studies on some integral stiffened plates.

6. R. L. POWELL and K. A. STETSON 1965 *Journal of the Optical Society of America* **55**, 1593–1598. Interferometric vibration analysis by wavefront reconstruction.